HHS Public Access

Author manuscript

Nat Immunol. Author manuscript; available in PMC 2018 March 01.

Published in final edited form as:

Nat Immunol. 2018 January ; 19(1): 76–84. doi:10.1038/s41590-017-0004-z.

Engagement of MHC class I by the inhibitory receptor LILRB1 suppresses macrophages and is a target of cancer immunotherapy

Amira A. Barkal[1], **Kipp Weiskopf**[1,2], **Kevin S. Kao**[1], **Sydney R. Gordon**[1], **Benyamin Rosental**[1], **Ying Y. Yiu**[1], **Benson M. George**[1], **Maxim Markovic**[1], **Nan G. Ring**[1], **Jonathan M. Tsai**[1], **Kelly M. McKenna**[1], **Po Yi Ho**[1], **Robin Z. Cheng**[1], **James Y. Chen**[1], **Layla J. Barkal**[3], **Aaron M. Ring**[4], **Irving L. Weissman**[1,5,6,7,*], and **Roy L. Maute**[1,8,*]

[1]Institute for Stem Cell Biology and Regenerative Medicine, Stanford University School of Medicine, Stanford, CA, USA

[2]Brigham and Women's Hospital, Boston, MA, USA

[3]Department of Biomedical Engineering, University of Wisconsin-Madison, Madison, WI, USA

[4]Department of Immunobiology, Yale University School of Medicine, New Haven, CT, USA

[5]Ludwig Center for Cancer Stem Cell Research and Medicine, Stanford, CA, USA

[6]Stanford Cancer Institute, Stanford University School of Medicine, Stanford, CA, USA

[7]Department of Pathology, Stanford University School of Medicine, Stanford, CA, USA

Abstract

Exciting progress in the field of cancer immunotherapy has renewed the urgency of the need for basic studies of immunoregulation in both adaptive cell lineages and innate cell lineages. Here we found a central role for major histocompatibility complex (MHC) class I in controlling the phagocytic function of macrophages. Our results demonstrated that expression of the common MHC class I component β_2-microglobulin (β2M) by cancer cells directly protected them from

*Correspondence and requests for materials: should be addressed to I.L.W. or R.L.M.: irv@stanford.edu; rmaute@stanford.edu.

[8]Present address: Ab Initio Biotherapeutics, South San Francisco, CA, USA. Amira A. Barkal, Kipp Weiskopf, Irving L. Weissman and Roy L. Maute contributed equally to this work.

Author contributions

A.A.B., K.W., I.L.W. and R.L.M. wrote the manuscript; A.A.B., K.W., A.M.R., I.L.W. and R.L.M. conceived of and designed all experiments; K.W. and R.L.M. performed LegendScreen analysis of tumor cell lines; K.S.K., S.R.G., B.M.G. and R.Z.C. assisted with mouse experiments; B.R. and Y.Y.Y. performed receptor-Fc staining experiments; M.M. assisted with tumor measurements and injections and provided sample preparation for primary human macrophages; N.G.R. generated human macrophages and tested the *in vitro* growth kinetics of DLD1 sublines; J.M.T. performed histology and immunofluorescence staining; K.M.M. generated NSG macrophages; K.M.M., P.Y.H. and R.L.M. tested CD47 expression in tumor cell lines; J.Y.C. assisted with generating knockout cell lines; L.J.B. assisted with statistical analysis; A.M.R. generated Fab fragments of W6/32; and I.L.W. supervised the research and edited the manuscript.

Competing interests

K.W., A.M.R., I.L.W. and R.L.M. and are co-inventors on patent application PCT/US2015/057233, which is related to this work, and own stock of FortySeven, which is pursing clinical approval of antibody Hu5F9-G4, directed against human CD47.

Supplementary information is available for this paper at https://doi.org/10.1038/s41590-017-0004-z.

phagocytosis. We further showed that this protection was mediated by the inhibitory receptor LILRB1, whose expression was upregulated on the surface of macrophages, including tumor-associated macrophages. Disruption of either MHC class I or LILRB1 potentiated phagocytosis of tumor cells both *in vitro* and *in vivo*, which defines the MHC class I–LILRB1 signaling axis as an important regulator of the effector function of innate immune cells, a potential biomarker for therapeutic response to agents directed against the signal-regulatory protein CD47 and a potential target of anti-cancer immunotherapy.

When properly stimulated, effector cells of both the innate immune system and adaptive immune system possess the ability to attack cancer cells. Clinical successes have highlighted the potential of this approach, but more complete understanding of immunoregulation is critical for the development of new therapeutic strategies.

Tumor-binding antibodies have been used in the clinic to treat many cancers, including lymphomas, breast cancer and colon cancer, among others[1]. These antibodies often exhibit multiple modes of action, but their efficacy is linked, in part, to their ability to stimulate antibody-dependent cellular phagocytosis of cancer cells[2]. However, the potency of this response is dampened by the expression, on the surface of cancer cells, of the signal-regulatory protein CD47, which engages the inhibitory receptor SIRPα on macrophages and functions as an anti-phagocytic ‘don’t eat me’ signal[3,4].

Therapeutic blockade of the CD47–SIRPα interaction greatly increases the antibody-induced phagocytosis of cancer cells both *in vitro* and *in vivo*[5–8]. Biological agents directed against this axis are currently in clinical trials for multiple indications and represent a promising immunotherapeutic strategy[9]. However, redundant inhibitory signals are commonplace in immunoregulation, and the CD47–SIRPα axis is probably not the only important therapeutic target for engaging macrophages to attack cancer cells. In order to identify additional regulators of these cells, we undertook a targeted screen for cancer-relevant ‘don’t eat me’ signals. Through this screen, we identified major histocompatibility complex (MHC) class I as a critical regulator of the effector function of macrophages within the tumor microenvironment.

Results

Expression of MHC class I correlates with resistance to phagocytosis

Drugs targeting the CD47–SIRPα pathway have broad efficacy in inducing the phagocytosis of cancer cells, yet some cells exhibit intrinsic resistance largely independent of disease subtype or tissue of origin[5–8]. To investigate this phenomenon further, we assessed the phagocytosis, by primary human macrophages, of a diverse panel of human cancer cell lines. Phagocytosis was quantified by a flow cytometry–based assay validated by cell-sorting experiments[8,10] and high-throughput microscopy (Supplementary Fig. 1). We found that the clinical-stage CD47-blocking antibody Hu5F9-G4 (anti-CD47)[11] significantly increased phagocytosis of the majority of cancer cell lines tested (Fig. 1a). However, despite the broad efficacy of this antibody, some cancer cell lines were not significantly phago-cytosed after treatment with anti-CD47, and among the responding cell lines, the magnitude of induced

phagocytosis varied widely (Fig. 1a). These differences did not correlate with cancer subtype, nor did they correlate with surface expression of CD47, which was high in all cell lines tested (Supplementary Fig. 2a). Anti-CD47 induces phagocytosis both by blocking CD47–SIRPα signaling and by opsonizing cells via its functional immunoglobulin G4 crystallizable fragment (Fc) and thereby providing an 'eat me' signal that activates Fc receptors on macrophages. We therefore speculated that the anti-CD47-resistant lines probably expressed one or more co-dominant inhibitory signals in addition to CD47.

In order to identify those signals, we used an antibody array system to characterize the surface immunophenotype of five cell lines that spanned a broad spectrum of human tumor types and a wide range of sensitivity to phagocytosis after treatment with anti-CD47 (Hu5F9-G4): the colon-cancer lines DLD1 and HCT116; the small-cell lung-cancer lines NCI-H82 and NCI-H196; and the pancreatic neuroendocrine tumor line APL1 (ref. [12]). In analyzing the data from these arrays, we identified a putative relationship between high expression of MHC class I proteins and resistance to anti-CD47-induced phagocytosis by macrophages (Supplementary Fig. 2b).

HLA α-chains and β_2-microglobulin (β2M) assemble to form the MHC class I complex[13], which has well-studied and essential roles in the regulation of T cells and natural killer (NK) cells but a comparatively limited function described for the regulation of macrophages[14,15]. Nonetheless, analysis of HLA expression across our broader panel of 18 cancer cell lines revealed a highly significant correlation between overall levels of MHC class I and resistance to macrophage-mediated phagocytosis (Fig. 1b). We observed no discernable relationship between the particular HLA phenotype of the cell lines and their sensitivity to phagocytosis (Supplementary Table 1). This correlation raised the possibility that expression of MHC class I is directly protective against macrophage attack.

MHC class I directly protects cells from macrophage attack

In order to investigate the functional implications of the correlation noted above, we undertook a series of genetic experiments using two lines from our 'discovery panel': APL1 and DLD1. These lines were chosen because both are highly positive for expression of CD47, but APL1 cells naturally have high expression of MHC class I, while DLD1 cells are negative for surface expression of MHC class I due to biallelic inactivation of the *B2M* locus[16]. Through stable genome engineering and sequential rounds of sorting by flow cytometry, we generated polyclonal sub-lines of both APL1 cells and DLD1 cells with all four permutations of positive or negative expression of MHC class I and CD47 (Fig. 2a,b).

Co-culture of those lines with donor-derived human macrophages revealed that in the absence of further stimulation, deletion of surface MHC class I was sufficient to modestly but significantly increase spontaneous phagocytosis in some cases (Fig. 2c). We further found that MHC class I–negative ($MHCI^-$) cells were significantly more sensitive to anti-CD47-induced phagocytosis than were their $MHCI^+$ counterparts (Fig. 2c,d). After being treated with an independent opsonizing antibody, cells lacking expression of both CD47 and MHC class I were the most sensitive to phagocytosis, while expression of either MHC class I or CD47 or expression of both simultaneously provided significant protection against

macrophage attack (Fig. 2e,f). Thus, our data demonstrated that MHC class I and CD47 were independent anti-phagocytic signals that might also work cooperatively.

To extend those results, we generated a Fab fragment from a monoclonal antibody that blocks HLA-A, HLA-B and HLA-C[17,18]. Consistent with our expectations, blockade via the HLA-binding Fab in absence of antibody Fc had no effect on the phagocytosis of the MHCI^{-} cell line DLD1 (Fig. 2g). However, when applied to a panel of MHCI^{hi} cells (Supplementary Fig. 2c), the HLA-binding Fab significantly increased anti-CD47-induced phagocytosis for four of six lines tested (Fig. 2f). Some cell lines (U2OS and SAOS2) were still resistant to phagocytosis after simultaneous blockade of CD47, blockade of MHC class I and opsonization (Fig. 2g), which suggested that such cells probably expressed additional anti-phagocytic signals.

LILRB1 detects MHC class I and suppresses phagocytosis

In order to further investigate the phenomenon of the inhibition of macrophage phagocytosis by MHC class I, we sought to identify the receptor or receptors involved in the detection of MHC. Monocyte-lineage cells have been reported to express various MHC-binding proteins, notably members of the LILR family[19,20]. Structural studies suggest that two members of this family, LILRB1 and LILRB2, bind MHC class I and also contain immunoreceptor tyrosine-based inhibitory motifs involved in the intracellular transduction of inhibitory signaling[20,21], which establishes them as strong candidates for MHC class I–mediated suppression of phagocytosis.

Analysis of human peripheral blood monocytes from four independent donors revealed that in addition to SIRPα, LILRB1 was expressed on the majority of monocytes, with only a subset being LILRB2^{+} (Fig. 3a,b). Primary mature macrophages from normal human spleen were positive for SIRPα expression, and approximately one third of the cells were LILRB1^{+}; nearly all cells were LILRB2^{-} (Fig. 3a,b). In primary macrophages isolated from ascites fluid of patients with ovarian carcinoma, expression of both SIRPα and LILRB1 was uniformly positive and very high; in contrast, there was minimal expression of LILRB2 (Fig. 3a,b). In tumor-associated macrophages from primary human colon carcinomas, we similarly saw higher expression of LILRB1 than of LILRB2 (Fig. 3a,b). We observed no significant difference between M1-like tumor-associated macrophages and M2-like tumor-associated macrophages in their expression of LILRB1 or LILRB2 and detected no expression of either LILRB1 or LILRB2 by non-immune tumor cells (Supplementary Fig. 3a,b). The pattern of high expression of LILRB1 but low expression of LILRB2 was also replicated by *ex vivo*–differentiated primary macrophages (Supplementary Fig. 3c,d), which suggested that our *in vitro* experiments correctly reflected the expression profile of tumor-associated macrophages.

On the basis of those observations, we investigated whether direct blockade of LILRB1 could increase the phagocytosis of MHCI^{+} cells. Indeed, we found that treatment with a blocking monoclonal antibody to LILRB1 (ref. [22]) significantly increased the anti-CD47-induced phagocytosis of MHCI^{+} cells but not that of their MHCI^{-} counterparts (Fig. 3c and Supplementary Fig. 3e). As expected on the basis of the low or negative expression of LILRB2 by mature macrophages, treatment with an LILRB2-blocking antibody[23] had no

significant effect on the phagocytosis of either MHCI^{+} cells or MHCI^{-} cells (Fig. 3c and Supplementary Fig. 3e).

In order to further investigate that relationship, we optimized and implemented a protocol to genetically modify the expression of LILRB1 in primary *in vitro*–derived human macrophages using the CRISPR–Cas9 ribonucleoprotein system. We observed a 42% reduction in population-wide expression of LILRB1 48 h following nucleofection with single guide RNA (sgRNA) targeting the *LILRB1* locus, relative to its expression in cells treated with the control sgRNA (Supplementary Fig. 3f). The corresponding knockout of *LILRB1* in nearly 50% of alleles was confirmed through the use of TIDE software for quantitative assessment of genome editing[24] (Supplementary Fig. 3g). In the presence of anti-CD47-mediated blockade, *LILRB1*-null macrophages demonstrated significantly greater phagocytic ability than that of macrophages treated with the off-target control sgRNA (Fig. 3d), which further demonstrated that the elimination of surface LILRB1 was sufficient to potentiate the phagocytosis of MHCI^{+} cells *in vitro*.

Together these data identified LILRB1—and largely excluded the possibility of involvement of LILRB2—as a primary mediator of repressive MHC class I signaling in many human macrophage populations, especially in the context of cancer immunotherapy.

β2M confers species-specific protection against macrophages

The assays reported above used cells derived from multiple independent macrophage donors, with no prior analysis or matching between macrophages and cancer cells on the basis of HLA haplotype, which suggested a much broader mechanism for the detection of MHC class I by LILRB1 than that of the mostly allele-specific mechanisms employed by T cells and NK cells[25–27]. Consistent with that, examination of the previously solved crystal structure of LILRB1 bound to the human MHC class I complex[20] revealed that the majority of contact residues between LILRB1 and MHC class I were within the invariant β2M subunit[28] rather than the highly polymorphic HLA α-chain (Fig. 4a). Alignment of the human and mouse β2M protein sequences revealed an identity mismatch of approximately 30%, including several key amino acids in the region of predicted contact between human β2M and proteins of the LILRB family (Fig. 4a, inset), which led us to hypothesize that these residues might be involved in species-specific signaling to macrophages.

Mouse β2M is unable to form stable complexes with human HLA α-chains; transgenic expression of the gene encoding mouse β2M in human β2M^{-} cells led to only low surface expression of MHC class I, as measured by an HLA-A-, HLA-B- and HLA-C-binding antibody (Supplementary Fig. 4). To circumvent that limitation, we generated a chimeric β2M in which the human β2M protein was altered to include the amino acids of mouse sequence only within the predicted region of interaction with proteins of the LILRB family (Fig. 4a, inset). Expression of the chimeric β2M in either β2M^{-} parental DLD1 cells or in APL1 cells with deletion of *B2M* enabled robust surface expression of HLA comparable to that achieved with fully human β2M protein (Fig. 4b). However, unlike cells expressing fully human MHC class I, these chimeric MHC class I cells no longer interacted with an LILRB1–Fc fusion protein (Fig. 4b), which suggested that they would probably no longer be

efficiently protected from phagocytosis and raised the possibility that chimeric MHC class I complexes might, conversely, be recognized by mouse macrophages.

We confirmed that although expression of fully human β2M strongly protected target cells against phagocytosis by human macrophages (Fig. 4c), it was less efficient in protecting the target cells against mouse macrophages (Fig. 4c); in contrast, expression of chimeric β2M offered a more-efficient protection against mouse macrophages than against human macrophages (Fig. 4c). Thus, the amino acid substitutions of the chimeric β2M had switched the species-specific bias of this signaling interaction. This genetic analysis suggested that the amino acid residues in the LILRB-interacting region of β2M were critical for the detection of MHC class I by both human macrophages and mouse macrophages.

MHC class I protects cells from macrophage attack *in vivo*

Mice of the non-obese diabetic–severe combined immunodeficiency strain with homozygous deficiency in the gene encoding the common γ-chain (*Il2rg*$^{-/-}$) (NSG mice) produce functional cells of the myeloid lineage, but lack T cells, B cells and NK cells and therefore can efficiently accept human cellular transplants[29]. We injected either MHCI^{-} tumor cells or human–mouse chimeric MHCI^{+} tumor cells (with all cells engineered to express green fluorescent protein, and with the MHCI^{-} population further engineered to express red fluorescent protein for the analyses in Fig. 5d only) subcutaneously into NSG mice and used quantitative *in vivo* bioluminescent imaging to follow tumor growth. After several weeks, chimeric MHCI^{+} tumors had grown significantly larger than MHCI^{-} tumors had (Fig. 5a); this growth difference ultimately manifested as a significant survival advantage for mice engrafted with MHCI^{-} tumors (Fig. 5b).

We also injected a mixed population of cells composed of 50% MHCI^{-} cells and 50% human–mouse chimeric MHCI^{+} cells into host mice and followed the evolution of these tumors over time. Tumors initially contained an approximately equal frequency of MHCI^{+} cells and MHCI^{-} cells (Fig. 5c,d, pre-injection and day 7), but after several weeks of growth, the tumors had become almost uniformly MHCI^{+}, as measured by flow cytometry (Fig. 5c,d, day 28). Whole-mount fluorescence microscopy of tumors showed an even distribution of MHCI^{-} cells and MHCI^{+} cells at early time points, but this gave way to a punctate distribution of only small clusters of MHCI^{-} cells by 14 d or 28 d (Fig. 5e), consistent with selective pressure by macrophages against the MHCI^{-} cells.

The sub-lines assessed above had no measurable cell-autonomous differences in proliferation (Supplementary Fig. 5a). Furthermore, expression of fully human MHC class I, rather than human–mouse chimeric MHC class I, provided no significant growth advantage relative to the growth of MHCI^{-} cells *in vivo* (Supplementary Fig. 5b). Along with the fact that NSG mice lack all immune cell subsets classically considered the main sensors of MHC class I (for example, T cells or NK cells) and that we readily observed phagocytosis of tumor cells by macrophages, via histology (Supplementary Fig. 5c), these results supported the proposal of a macrophage-mediated, MHC class I–driven immunosurveillance mechanism.

In order to determine whether the protection against phagocytosis and tumor growth conferred by the chimeric MHC class I complex could also be recapitulated in a syngeneic

mouse system, we generated stable lines of the mouse melanoma B16-F10 with all four permutations of positive or negative expression of mouse MHC class I and CD47 (Fig. 6a) and engrafted them into lymphocyte-deficient (*Rag2*$^{-/-}$*Il2r*g$^{-/-}$) mice. After 20 d of *in vivo* growth, there was no significant difference between the volume of β2M^{-} tumors and that of CD47^{-} tumors (Fig. 6b). However, tumors lacking both β2M and CD47 grew significantly less than wild-type tumors did (Fig. 6b). Given that *Rag2*$^{-/-}$*Il2r*g$^{-/-}$ hosts lack NK cells, innate lymphoid cells and T cells, this effect served as demonstration of a macrophage-mediated, MHC class I–regulated anti-tumor effect.

We next sought to investigate the therapeutic potential of antagonizing the signaling axis noted above in an immunocompetent *in vivo* model. In contrast to studies of lymphocyte-free models, studies of immunocompetent hosts can elucidate the contributions of additional cell types such as T cells and NK cells and can serve as a system with which to investigate communication and supportive signaling between the adaptive immune system and innate immune system. In order to parse the individual anti-tumor effects of macrophages and NK cells, we compared the engraftment and growth of wild type, *B2m*$^{-/-}$, *Cd47*$^{-/-}$ and *B2m*$^{-/-}$*Cd47*$^{-/-}$ B16-F10 tumors in fully immunocompetent hosts and wild-type hosts depleted of NK cells or macrophages.

At 25 d after engraftment, we observed that the growth of wild-type B16-F10 tumors was significantly greater after depletion of either NK cells or macrophages (Fig. 6c), which demonstrated that both cell types contributed to anti-tumor immunity in this model. We hypothesized that although deletion of *B2m* might sensitize tumor cells to killing by either NK cells or macrophages, it also liberated them from detection and killing mediated by the T cell antigen receptor. Indeed, we found that tumors in which *B2m* was deleted grew larger than did wild-type tumors and were not significantly affected by depletion of either macrophages or NK cells (Fig. 6c). In contrast, for tumors in which both *B2m* and *Cd47* were deleted, depletion of macrophages significantly reduced anti-tumor immunity and led to increased tumor growth, but depletion of NK cells did not (Fig. 6c).

We also compared the engraftment and growth of *B2m*$^{-/-}$, *Cd47*$^{-/-}$ and *B2m*$^{-/-}$*Cd47*$^{-/-}$ B16-F10 tumors in fully immunocompetent hosts with that in *Ccr2*$^{-/-}$ hosts, which are specifically defective in the tumor-homing activity of monocyte-derived macrophages. We observed no significant difference in the engraftment or growth of wild type B16-F10 cells in immunocompetent hosts relative to their engraftment and growth in *Ccr2*$^{-/-}$ hosts, but *B2m*$^{-/-}$, *Cd47*$^{-/-}$ and *B2m*$^{-/-}$*Cd47*$^{-/-}$ tumors showed significantly greater engraftment and growth in the *Ccr2*$^{-/-}$ hosts than in immunocompetent hosts (Supplementary Fig. 6a). Together these findings confirmed an important macrophage-mediated role for MHC class I signaling and, together with our *in vitro* data, supported the proposal of cooperativity of the MHC class I and CD47 signaling axes.

In addition to assessing net effects on tumor mass, we were able to investigate the effect of deletion of *B2m* and *Cd47* on the infiltration of a variety of subpopulations of immune cells in surviving mice. Analysis of dissociated tumors from immunocompetent hosts by flow cytometry demonstrated that specifically in *B2m*$^{-/-}$ *Cd47*$^{-/-}$ tumors, there was increased infiltration of all varieties of immune cells assessable by our marker panel. In particular, this

increase included immune cells involved in the adaptive immune response, such as T cells and dendritic cells (Fig. 6d; gating strategy, Supplementary Fig. 6e). Critically, these effects were abolished by depletion of macrophages (Fig. 6d), suggestive of an important immunoregulatory role for these cells in the tumor microenvironment that was influenced by signaling via MHC class I and CD47 to macrophages. Elimination of multiple 'don't eat me' signals might thus lead macrophages to promote a robust shift toward a more immunogenic, anti-tumor phenotype.

The polarization of macrophages to either an inflammatory, M1, 'anti-tumor' state or anti-inflammatory, M2, 'pro-tumor' state has an important role in the net effect of macrophages on the tumor microenvironment[30], and we hypothesized that inhibitory signaling through LILRB1 might contribute to a tumor-promoting macrophage phenotype. Analysis by flow cytometry revealed that deletion of *LILRB1* from macrophages *in vitro* resulted in a significantly greater abundance of cells with an M1-like surface profile than that among macrophages treated with an off-target control sgRNA (Supplementary Fig. 6b). Given that we observed this shift in the absence of non-macrophage cells, this result was consistent with a possible role either for *in cis* LILRB1–MHC class I signaling or perhaps signaling between LILRB1 and MHC class I on adjacent macrophage cells in culture.

Discussion

The data presented here have demonstrated MHC class I to be a regulatory signal for the effector functions of macrophages and have thus expanded the understanding of one of immunology's best-studied and most important signaling complexes, and have also highlighted the central role of MHC class I in coordinating the activity of both the adaptive immune system and the innate immune system. MHC class I–LILRB1 signaling has been previously studied in a subset of NK cells[17,31,32], and it has been studied in the myeloid lineage for its role in monocyte activation[19]. Our data suggest that the regulation of phagocytosis by macrophages is an additional key role of LILRB1 signaling. LILRB1 recognizes a wide variety of HLA haplotypes[33] due to its interaction with the invariant β2M subunit of MHC class I[20], which suggests that this signaling axis is relevant across diverse patient populations.

Although we were able to demonstrate that the MHC class I–to–macrophage signaling axis was active in both immunocompromised mice and immunocompetent mice, in our current work we did not identify the functional equivalent of human LILRB1 in mouse macrophages. Several candidates, including the mouse receptor PirB, have been reported to bind MHC class I[34] and have expression patterns in immune cells consistent with a LILRB1-like function. However, full characterization of the mouse system will be an important step in understanding signaling via MHC class I to macrophages during normal immunity and in the tumor microenvironment.

Our results have important implications for several aspects of macrophage biology. Viruses can avoid the presentation of foreign peptides to T cells by the downregulation of surface MHC class I, which can consequently activate NK cell attack due to lack of binding of MHC by killer-cell immunoglobulin-like receptors[35]. We hypothesize that the MHC class I–

LILRB1 signaling axis might serve a similar role in the immunosurveillance of infected cells. Consistent with our hypothesis, the human cytomegalovirus (CMV) family has evolved to encode a protein, UL-18, that structurally mimics the MHC class I α-chain but prevents binding by T cells[20]. It binds LILRB1 with > 1,000-fold higher affinity than do native MHC complexes and, according to published reports, inhibits the subset of NK cells that express LILRB1 (ref. [32]). Given the high expression of LILRB1 in mature macrophages, UL-18 probably similarly modulates the macrophage-mediated phagocytosis of CMV-infected cells, which might influence the pathology of CMV infection.

MHC class I–LILRB1 signaling is also probably important in the dynamics of programmed cell removal. As erythrocytes age, their effective CD47 signaling gradually decreases and eventually drops below a critical threshold, which enables the phagocytosis of red blood cells by macrophages[4,36]. The majority of normal human cells, including erythrocyte precursors, express MHC class I, but mature red blood cells lack or have considerably diminished surface expression of this protein. This loss of MHC class I during erythrocyte differentiation might serve to explain the potent erythrophagocytosis and transient anemia induced by anti-CD47 or CD47-binding Fc fusion proteins when used as cancer therapy[7,8].

As demonstrated by our results both *in vitro* and *in vivo*, loss of MHC expression sensitized cancer cells to macrophage attack. Many cancers exhibit compromised or absent expression of surface MHC[37,38] and, due to the resulting impaired presentation of cancer neo-antigens, patients with such cancers might be poor candidates for T cell–focused therapies. However, our results suggest that they might in fact be the ideal candidates for macrophage-mediated immunotherapy, and thus while low MHC expression might be used as a negative biomarker for the efficacy of T cell–focused therapies, it might instead be a positive biomarker for the efficacy of anti-CD47 or anti-SIRPα drugs in development. SIRPα and LILRB1 also show variable expression in primary patient macrophages, probably due to variable conditions of immunological and inflammatory signaling, and might themselves be useful biomarkers.

In patients with tumors that have normal or high expression of MHC class I, agents directed against the MHC class I–LILRB1 axis might facilitate an anti-tumor immune response and could potentially act together with agents directed against CD47 or SIRPα. Like CD47, MHC class I is ubiquitously expressed by normal cells; in considerations of this axis as a therapeutic target, key questions arise about safety and specificity. To this point, we note that apart from depletion of MHCI^{-} erythrocytes, which would not be further exacerbated by blockade of MHC class I–LILRB1 signaling, toxicity in normal tissues has thus far not been reported for anti-CD47 agents in animal models[7,8]. This is despite the fact that some normal cells, such as those of the central nervous system, have low expression of MHC class I. We also note that *B2m*$^{-/-}$ mice have been reported to present few if any phenotypes that are attributable to the attack of normal cells by macrophages[39,40]. Finally, our *in vitro* experiments demonstrated that some cell lines (U2OS and SAOS2) remained highly resistant to phagocytosis even after simultaneous blockade of both CD47–SIRPα and MHC class I–LILRB1 signaling, a result potentially consistent with the expression of additional, as-yet-unidentified ‘don’t eat me’ signals. Normal tissues might similarly express such redundant signals. Nonetheless, careful evaluation of macrophage-mediated autoimmune responses will be a critical subject of future work on this signaling axis.

The immunotherapy field has been energized by the tremendous success of T cell–mediated anti-cancer treatments, and the innate immune system presents a substantial future therapeutic opportunity. Macrophage antibody-dependent cellular phagocytosis can increase the cross-presentation of tumor antigens to T cells and might thereby enhance the potency of an adaptive anti-tumor immune response[41]. Our results indicate that blocking both the MHC class I–LILRB1 signaling axis and CD47–SIRPα signaling axis might sensitize tumors to macrophage attack and might indirectly enhance the function of other immune cells. If properly applied, agents directed against the MHC class I–LILRB1 signaling axis might be an important component of therapeutic regimens that aim to engage the key effector functions of macrophages.

Methods

Cell culture

All cell lines were obtained from ATCC with the exception of APL1, which was a gift from G. Krampitz (Stanford University)[12]. DLD-1, NCI-H69, NCI-H82, NCI-H1688, NCI-H196, NCI-H524, Bon and APL1 cells were grown in RPMI + GlutaMax (Life Technologies) supplemented with 10% FBS (Hyclone) and 100 U/ml penicillin and streptomycin (Life Technologies). NCI-H128 cells were grown in RPMI + GlutaMax (Life Technologies) supplemented with 20% FBS (Hyclone) and 100 U/ml penicillin and streptomycin (Life Technologies). HT-29, SkBr3 and SkMel3 cells were grown in McCoy's 5A + GlutaMax (Life Technologies) supplemented with 10% FBS (Hyclone), and 100 U/ml penicillin and streptomycin (Life Technologies). LS-174T, MCF7 and SkMel28 cells were grown in Eagle's Minimum Essential Media (ATCC) supplemented with GlutaMax (Life Technologies), 10% FBS (Hyclone) and 100 U/ml penicillin and streptomycin (Life Technologies). When necessary, cells were detached from plates and disaggregated using TrypLE Express (Life Technologies) according to the manufacturer's indications. Unless otherwise indicated, cell lines were propagated and subcultured according to ATCC guidelines.

Generation of lentiviral particles

HIV-based replication-incompetent lentiviral particles were generated in 293 Lenti-X cells (Clontech) by co-transfection of pMDG.2 vector (Addgene), psPAX2 (Addgene) and a third vector specific to the lentiviral application, using the Xtremegene HD transfection reagent (Roche) according to the manufacturer's protocol. Vectors were transfected at a mass ratio of 4:2:1, lenti-specific vector:psPAX2:pMDG.2. After transfection, cell culture media supernatant was collected at 36 h and 60 h. Lentiviral particles were concentrated either by ultracentrifugation for 2.5 h at 50,000*g* or with PEG-it (Systems Biosciences) according to the manufacturer's indications. Proper biosafety and disposal techniques were followed whenever using lentiviral reagents, according to Stanford University guidelines.

Generation of DLD1 and APL1 cell sub-lines

In order to generate sub-lines of DLD1 and APL1 cells, parental, unmodified cells were harvested in single-cell suspensions and were mixed with pre-warmed growth media, concentrated lentivirus and 10 μg/ml polybrene (Sigma). Cells were then centrifuged at

1,800 r.p.m., room temperature for 45 min. Lentiviral pools included at least three distinct viral species: one encoding the Cas9 nuclease, and two others encoding different CRISPR small guide RNAs (sgRNAs) targeting the first exon of either *CD47* or *B2M*, as appropriate. CRISPR sgRNAs were designed using online tools (http://genome-engineering.org) and were of the following sequences: sgCD47-1: GCTACTGAAGTATACGTAAAG, sgCD47-2: GCTTGTTTAGAGCTCCATCAA, sgβ2M-1: GAGTAGCGCGAGCACAGCTA, sgβ2M-2: GGCCGAGATGTCTCGCTCCG. 7 d after infection, cells were assessed for expression status by flow cytometry. CD47 was assessed by staining with APC-conjugated B6H12 (Biolegend), and HLA-A, HLA-B and HLA-C was assessed by staining with PE-Cy7-conjugated W6/32 (Biolegend). Cells were sorted on a FACSAria II cell sorter (BD Biosciences). Typically, each cell line was sorted three times, separated by several days of recovery and expansion between rounds. Wild-type human *B2M* (NC_000015.10), wild-type mouse *B2m* (NC_000068.7), or chimeric human–mouse *B2M* (hmcβ2M; sequence below) were cloned into the NheI and NotI sites of the pCDH-CMV-MCS-EF1-Puro vector (Systems Biosciences), and these vectors were used to produce lentivirus and introduce transgenes, as appropriate. DLD1-Δ(CD47) was generated by transient co-transfection of CD47-targeting TALEN vectors, described below, using Xtremegene HD (Roche) according to the manufacturer's indicated protocol. All other genetic modifications were induced using lentiviral delivery of transgenes, or lentiviral delivery of *Cas9* and corresponding sgRNAs, as described above.

TALEN design and construction

TALENs were designed and assembled as described[29]. The genomic locus of human *CD47* (NC_000003.12) was scanned for putative TALEN binding pairs. Exon 2 was ultimately selected for targeting and the TALEN pairs TGTCGTCATTCCATGCTTTG and TATACTTCAGTAGTGTTTTG were respectively cloned into the pTALEN backbone.

GFP-luciferase and RFP-luciferase transduction

In order to facilitate both the flow cytometry–based phagocytosis assay and *in vivo* imaging, we generated sublines of DLD1, HT-29, LS-174T, SkBr3, Bon, APL1, SkMel28 and SkMel3 cells engineered via lentiviral infection to stably express a green fluorescent protein (GFP)–luciferase fusion protein (Systems Biosciences, catalog number BLIV100PA/VA-1). U2OS and SAOS2 were engineered via lentiviral infection to stably express a red fluorescent protein (RFP)–luciferase fusion protein (Systems Biosciences, catalog number BLIV101PA/VA-1). The MHCI-APL1 cells used in Fig. 5d were engineered to express both GFP-luciferase and RFP-luciferase with the vectors described above. Parental cells were harvested in single-cell suspensions and were mixed with pre-warmed growth medium, concentrated lentivirus and 10 μg/ml polybrene (Sigma). Cells were then centrifuged at 1,800 r.p.m., room temperature for 45 min. Uniform GFP^+ or RFP^+ populations were then generated by sequential rounds of cell sorting on a FACSAria II cell sorter (BD Biosciences).

Macrophage generation

Leukocyte reduction system (LRS) chambers from anonymous donors were obtained from the Stanford Blood Center. Monocytes were purified from these samples on an autoMACS

Pro Separator (Miltenyi) using anti-CD14 microbeads optimized for whole-blood separation (Miltenyi) according to the manufacturer's suggested protocol. Monocytes were then differentiated to macrophages by 7–10 d of culture in IMDM + GlutaMax (Life Technologies) supplemented with 10% AB Human Serum (Life Technologies) and 100 U/ml penicillin and streptomycin (Life Technologies). NSG macrophages were generated as previously described[17]. In brief, bone marrow cells were harvested from the lower limbs of 6- to 8-week-old NSG mice, and were cultured for 7 d in IMDM + GlutaMax[13] (Life Technologies) supplemented with 10% FBS (Hyclone), 100 U/ml penicillin and streptomycin and 10 ng/ml murine M-CSF (Peprotech).

Flow cytometry–based phagocytosis assay

Each phagocytosis reaction reported in this work was performed by co-culture of 100,000 target cells and 50,000 macrophages for 2 h in ultra-low-attachment 96-well U-bottom plates (Corning) in IMDM + GlutaMax (Life Technologies) without antibiotics or serum added. Macrophages were generated as described above and were harvested from plates using TrypLE Express (Life Technologies). Target cells were either engineered to stably express GFP or RFP, as described above, or were stained with Calcein AM (Life Technologies) according to the manufacturer's indications before co-culture. Treatment antibodies, including anti-CD47 (clone Hu5F9-G4, cetuximab, Bristoll-Myers Squibb), anti-LILRB1 (clone GHI/75, BioLegend) and anti-LILRB2 (clone 27D2, Biolegend) were added to reactions at a concentration of 10 μg/ml. After co-culture, reactions were stained were stained with APC-labeled anti-CD45 (clone HI30, BioLegend) to identify human macrophages, and with PE-Cy7-labeled anti-F4/80 (clone BM8, BioLegend) to identify NSG mouse macrophages. DAPI staining was used to exclude dead cells from the analysis (Sigma). Reactions were run on an LSRFortessa Analyzer outfitted with a high-throughput auto-sampler (BD Biosciences). Phagocytosis was evaluated as a sum of the GFP^+ macrophages, expressed as a percentage of the total macrophages, as analyzed using FlowJo v.9.4.10 (Tree Star) and was normalized as indicated in the figure legends. Unless otherwise stated, each replicate represents a true biological replicate (i.e., an independent human macrophage donor), and unless otherwise indicated, replicates were split between a minimum of two independent experimental instances (for example, four independent donors evaluated on day 1, with an additional four independent donors evaluated on day 2). Sample size was chosen to ensure a greater than 95% probability of identifying, by the two-tailed *t*-test, an effect of > 20%, assuming a technical variation of 15%.

Antibody array

We used the LegendScreen antibody array system (BioLegend) to assess the surface phenotype of the NCI-H69, NCI-H82, NCI-H524 and NCI-H196 cell lines. The cells were harvested and disaggregated with TrypLE (Life Technologies), and NCI-H82 and NCI-H69 cells were stained using Calcein AM (Life Technologies) according to the manufacturer's protocol. NCI-H82 (calcein-stained) cells and NCI-H524 (unstained) cells were run together in a multiplex fashion, as were NCI-H69 (calcein-stained) cells and NCI-H196 (unstained) cells. Cells were distributed among antibody-containing wells, then were stained and washed according to the manufacturer's indications. Samples were subsequently run on an LSRFortessa Analyzer outfitted with a high-throughput auto-sampler (BD Biosciences).

Fluorescence levels were evaluated using FlowJo v.9.4.10 (Tree Star). Calcein staining signal was used to deconvolute multiplexed samples.

Antibody staining

Flow cytometry was performed either on a FACSAria II cell sorter (BD Biosciences) or on an LSRFortessa Analyzer (BD Biosciences). Surface CD47 was assessed by antibody staining with clone B6H12 (BioLegend) at a dilution of 1:100. HLA-A/B/C was assessed by antibody staining with clone W6/32 (BioLegend) at a dilution of 1:50. LILRB1 was assessed by antibody staining with clone GHI/75 (BioLegend) at a dilution of 1:25. LILRB2 was assessed by antibody staining with clone 27D2 (BioLegend) at a dilution of 1:25. The M1-like macrophage panel was as follows: $DAPI^{-}CD11b^{+}CD206^{-}CD64^{+}$. The M2-like macrophage panel was as follows: $DAPI^{-}CD45^{+}CD11b^{+}CD64^{-}CD206^{+}$. All stains were performed on ice for 30 min, then were washed and resuspended according to standard practice.

LILRB1-Fc staining

Cells were incubated with LILRB1-Fc or human Fc control (R&D Systems, 40 μg/ml) for 1.5 h at 4 °C, and washed and stained with APC-conjugated $F(ab')^2$ goat anti–human immunoglobulin G (Jackson, 109-136-098). Staining and washing buffer consisted of 0.2% (w/v) BSA and 0.05% sodium azide in PBS

Human-mouse chimeric β2M

Chimeric β2M was designed to incorporate C-terminal amino acid differences from mouse β2M into a primarily human β2M sequence. The sequence (indicated below) was chemically synthesized (IDT), and cloned into the NheI and NotI sites of pCDH-CMV-MCS-EF1-Puro. Sequence of mouse origin is in lower case.

>
hmcβ
2M_geneblockTTTAAGCTAGCATGTCTCGCTCCGTGGCCTTAGCTGTGCTCGCGCTA
CTCTCTCTTTCTGGCCTGGAGGCTATCCAGCGTACTCCAAAGATTCAGGTTTACTC
ACGTCATCCAGCAGAGAATGGAAAGTCAAATTTCCTGAATTGCTATGTGTCTGGG
TTTCATCCATCCGACATTGAAGTTGACTTACTGAAGAATGGAGAGAGAATTGAAA
AAGTGGAGCATTCAGACTTGTCTTTCAGCAAGGACTGGTCTTTCTATCTCTTGTAC
TACACTGAATTCACCCCCACTGAAAAAGATGAGTATGCCtgcagagttaagcatgccagtatggc
cgagcccaagaccgtctactgggatcgagacatgtgaGCGGCCGCAATTT

Generation of W6/32 Fab fragments

W6/32 antibody (BioXcell) was desalted into a solution of 20 mM sodium citrate, pH 6.0, 25 mM cysteine and 5 mM EDTA and was diluted to a concentration of 4 mg/ml. Protease digestion was achieved by mixing with 250 μl immobilized ficin resin (Thermo Scientific) per ml of antibody. The mixture was incubated with rotation at 37 °C for 5 h. After incubation, Fab fragments were purified from undigested antibody and Fc fragments were purified by ion-exchange chromatography with a monoQ column, followed by size-

exclusion chromatography with a Superdex-200 column. Fab fragments were quantified by Nanodrop, and checked for purity by Coomassie stain.

Crystal structure images

Crystal structure images were generated with MacPyMol v. 1.7.0.3 from a published structure (Protein Data Bank accession code IP7Q)[22].

Mice

Nod.Cg-Prkdc^{scid} IL2rg^{tm1Wjl}/SzJ (NSG) mice were used for all *in vivo* xenograft experiments. BALB/c *Rag2*$^{-/-}$ *IL2rg*$^{-/-}$ mice, B6.129(Cg)-*Ccr2*$^{tm2.1Ifc}$/J mice (Jackson Labs) and C57BL/6 mice (Jackson Labs) were used for B16 tumor models. Mice were engrafted with tumors at approximately 6–12 weeks of age, and experiments were performed with age- and sex-matched cohorts. Mice were maintained in a barrier facility under the care of the Stanford Veterinary Services Center and handled according to protocols approved by the Stanford University Administrative Panel on Laboratory Animal Care.

In vivo growth experiments

NSG mice were given subcutaneous injection into the right flank of 100,000 GFP-luciferase-labeled APL1-Δ(β2M) (30 mice) or APL1-Tg(hmcB 2M)-Δ(β2M) cells (30 mice) and were randomized into treatment cohorts using online list randomization tools (https://www.random.org/). Sample size was chosen to ensure a greater than 95% probability of identifying, by the two-tailed *t*-test, an effect of > 50%, assuming a technical variation of 50%. Starting on day 14, mice were treated once per week by intraperitoneal injection of either 100 μl of PBS or 250 μg Hu5F9-G4 at a concentration of 2.5 mg/ml. Tumor luminescence was measured once per week using an IVIS Spectrum imager (Perkin Elmer). Measurements were discontinued when tumors in a measurement group began to exceed 5×10^{10} total flux, which is, in our experience, a threshold above which bioluminescent signals are less accurate. Across additional experiments, including pilot experiments, additional mice were engrafted subcutaneously with these cell lines and treated with PBS but were not included as part of this data set. One additional cage of four mice was engrafted with each APL1-Δ(β2M) and APL1-Tg(hmcβ2M)-Δ(β2M) and received once-weekly Hu5F9-G4 treatment but were ultimately not included in the final analysis of the experiment. Mouse experiments were performed in a non-blinded fashion.

For B16 melanoma models, mice were engrafted with 500,000 melanoma cells in PBS. Tumor volumes were measured on day 15, day 20 or day 25, as indicated.

Macrophage- and NK cell–depletion studies

Female C57Bl/6J mice (Jackson Laboratory) were depleted of macrophages or NK cells by intraperitoneal injection of 400 μg CSFR-1 antibody (BioXCell, Clone AFS98) and 350 μg NK1.1 depleting antibody (BioXCell, Clone PK136), respectively, three times weekly with beginning 3 weeks before tumor implantation and continuing for the duration of the study. Non-depleted control animals were given intraperitoneal injection of PBS following the same dosing schedule. Macrophage depletion and NK depletion were verified separately by flow cytometry of peritoneal lavage, splenic cells, and peripheral blood, from a separate

cohort of mice at the time of tumor implantation. Macrophage-depleted, NK-depleted, and control mice were given subcutaneous injection of 1.5×10^5 of B16F10-WT, B16F10-Δβ2M, B16F10-ΔCD47 or B16F10-Δβ2M,CD47 cells into the lower dorsal region of the mouse. Beginning 2 weeks after tumor injection, tumor measurements were taken three times weekly. When tumors reached 20 mm in diameter, tissue was harvested to asses for infiltrating immune cells, including NK cells ($CD45^+TCR\beta^-NK1.1^+$) and mature macrophages ($CD45^+TCR\beta^-Gr1^{lo-neg}CD11b^+F4/80^+$) to ensure sufficient depletion.

Isolation of tumor-infiltrating immune cells

Mouse tumor samples were excised and incubated with 10 ml RPMI supplemented with 10 μg/ml DNase I (Sigma Aldrich) and 25 μg/ml Liberase (Roche) for 10–15 min at 37 °C. Tumors were homogenized by pipetting and filtering through a 100-μm nylon filter. Following the dissociation, 5×10^6 cells were pelleted and resuspended in FACS buffer and blocked with monoclonal antibody to CD16/32 (Trustain fcX, Biolegend) for 10 min before staining. All tumors were stained with anti-CD45 (Biolegend, Clone 30-F11), anti-TCRβ(BD, Clone H57-97), anti-NK1.1 (eBioscience, Clone PK136), anti-CD11b (Biolegend, Clone M1/70), anti-F4/80 (Biolegend, Clone BM8), anti-Ly6C (BD, Clone AL-21), anti-CD11c (Biolegened, Blone N418) and anti-Gr-1 (Biolegend, Clone RB6-8C5). Dead cells were eliminated from analysis by excluding $Hoechst^+$ cells. All samples were assayed using a FACSAria cell sorter (BD Biosciences), and channel compensations were performed using single-stained UltraComp eBeads (Affymetrix) or cells. Data were analyzed using FlowJo, and outliers in each group were removed using Prism Outlier Calculator (http://graphpad.com/quickcalcs/Grubbs1.cfm).

Macrophage genetic alteration

sgRNA molecules targeting the LILRB1 locus and off-target loci were purchased as modified, hybridized RNA molecules from Synthego. The sgRNA sequences were as follows: sgRNA LILRB1, 5′-GAGACCCUGACUCUGCAGUG-3′; and off-target sgRNA, 5′-AGGCCCCCUCCCAGGCGUAG-3′. Cas9-3NLS protein was purchased from IDT. Cas9 ribonucleoproteins were formed by incubatio of Cas9 protein and modified RNAs at a molar ratio of 1:2.5, respectively, at 37 °C for 30 min. Day 7, *in vitro*–derived human macrophages were electroporated with pre-formed ribonucleoprotein using the Lonza Nucleofector 4D and the P3 Primary Cell Nucleofction Kit (V4XP-3024). Following nucleofection, macrophages were cultured for an additional 48 h, after which genomic DNA was collected and INDEL frequencies were analyzed using TIDE (‘tracking of indels by decomposition’) software, as described previously[24]. Phagocytosis experiments were performed with biological replicates using macrophages from two human donors.

Histology

APL1 tumors were fixed in 2% paraformaldehyde overnight at 4 °C. Tissue was embedded and frozen in optimal cutting temperature compound O.C.T (Sakura) or embedded in paraffin. Frozen sections were cut at 4–7 μm and were saved for immunofluorescence.

Immunofluorescence

Immunofluorescence studies were performed on frozen sections. Frozen sections were thawed at room temperature for 10 min and washed in PBS twice. Slides were blocked in 5% serum for 30 min at room temperature. Sections were subsequently stained with primary antibodies to F4:80 (1:100, rat monoclonal, Abcam) overnight at 4 °C and were washed three times in PBS. Slides were stained were incubated with secondary antibodies conjugated to AlexaFluor 647 for 1–2 h at room temperature. Stains were washed once with PBST and three times with PBS before nuclear staining with Hoechst 33342 (Life Technologies), for 2 min, and were mounted with Fluoromount G (Southern Biotech). Basic photo processing, including fluorescence channel false-coloring, channel merge, and brightness and contrast adjustment were performed using Adobe Photoshop (Adobe).

Life Sciences Reporting Summary

Further information on experimental design and reagents is available in the Life Sciences Reporting Summary.

Data availability statement

The primary data underlying the flow cytometry and associated analyses for all figures and supplementary figures are available from the corresponding authors upon request.

Supplementary Material

Refer to Web version on PubMed Central for supplementary material.

Acknowledgments

We thank the members of the Weissman laboratory and the Stanford Stem Cell Center community for discussion and assistance; J.P. Volkmer, R. Majeti, K. Loh, N. Fernhoff, M. McCracken and J. Zee for input and advice; T. Storm, T. Naik, A. McCarty, F. Khameneh, J. Ho and P. Lovelace for logistical support; and G. Krampitz (Stanford University) for the APL1 cell line. Supported by the D.K. Ludwig Fund for Cancer Research (NIH R01CA086017 and NIHG R01GM100315 to I.L.W.), the Cancer Research Institute (Irvington Fellowship to R.L.M.), the Human Frontier Science Program Organization (postdoctoral fellowship to B.R.), the NIH (hematology training grant T32 HL120824-03 to B.R.), the University of Wisconsin Medical Scientists Training Program (GM008692 to L.J.B.), the National Research Service Award 1F30DK108561, the Paul and Daisy Soros Fellowship for New Americans (to J.M.T.) and the Stanford Medical Scientist Training Program (NIH GM07365 to A.A.B., K.W., A.M.R., J.M.T., B.M.G. and J.Y.C.).

References

1. Weiner LM, Dhodapkar MV, Ferrone S. Monoclonal antibodies for cancer immunotherapy. Lancet. 2009; 373:1033–1040. [PubMed: 19304016]
2. Weiskopf K, Weissman IL. Macrophages are critical effectors of antibody therapies for cancer. MAbs. 2015; 7:303–310. [PubMed: 25667985]
3. Jaiswal S, et al. CD47 is upregulated on circulating hematopoietic stem cells and leukemia cells to avoid phagocytosis. Cell. 2009; 138:271–285. [PubMed: 19632178]
4. Oldenborg PA, et al. Role of CD47 as a marker of self on red blood cells. Science. 2000; 288:2051–2054. [PubMed: 10856220]
5. Majeti R, et al. CD47 is an adverse prognostic factor and therapeutic antibody target on human acute myeloid leukemia stem cells. Cell. 2009; 138:286–299. [PubMed: 19632179]
6. Chao MP, et al. Anti-CD47 antibody synergizes with rituximab to promote phagocytosis and eradicate non-Hodgkin lymphoma. Cell. 2010; 142:699–713. [PubMed: 20813259]

7. Willingham S, et al. The CD47-SIRPa interaction is a therapeutic target for human solid tumors. Proc Natl Acad Sci USA. 2012; 109:6662–6667. [PubMed: 22451913]
8. Weiskopf K, et al. Engineered SIRPα variants as immunotherapeutic adjuvants to anticancer antibodies. Science. 2013; 341:88–91. [PubMed: 23722425]
9. Weiskopf K. Cancer immunotherapy targeting the CD47/SIRPα axis. Eur J Cancer. 2017; 76:100–109. [PubMed: 28286286]
10. Weiskopf K, et al. CD47-blocking immunotherapies stimulate macrophage-mediated destruction of small-cell lung cancer. J Clin Invest. 2016; 126:2610–2620. [PubMed: 27294525]
11. Liu J, et al. Pre-clinical development of a humanized anti-CD47 antibody with anti-cancer therapeutic potential. PLoS One. 2015; 10:e0137345. [PubMed: 26390038]
12. Krampitz GW, et al. Identification of tumorigenic cells and therapeutic targets in pancreatic neuroendocrine tumors. Proc Natl Acad Sci USA. 2016; 113:4464–4469. [PubMed: 27035983]
13. Bjorkman PJ, et al. Structure of the human class I histocompatibility antigen, HLA-A2. Nature. 1987; 329:506–512. [PubMed: 3309677]
14. Klein J, Sato A. The HLA system. First of two parts. N Engl J Med. 2000; 343:702–709. [PubMed: 10974135]
15. Klein J, Sato A. The HLA system. Second of two parts. N Engl J Med. 2000; 343:782–786. [PubMed: 10984567]
16. Bicknell DC, Rowan A, Bodmer WF. β2-microglobulin gene mutations: a study of established colorectal cell lines and fresh tumors. Proc Natl Acad Sci USA. 1994; 91:4751–4755. [PubMed: 8197130]
17. Borges L, Hsu ML, Fanger N, Kubin M, Cosman D. A family of human lymphoid and myeloid Ig-like receptors, some of which bind to MHC class I molecules. J Immunol. 1997; 159:5192–5196. [PubMed: 9548455]
18. Barnstable CJ, et al. Production of monoclonal antibodies to group A erythrocytes, HLA and other human cell surface antigens-new tools for genetic analysis. Cell. 1978; 14:9–20. [PubMed: 667938]
19. Fanger NA, et al. The MHC class I binding proteins LIR-1 and LIR-2 inhibit Fc receptor-mediated signaling in monocytes. Eur J Immunol. 1998; 28:3423–3434. [PubMed: 9842885]
20. Willcox BE, Thomas LM, Bjorkman PJ. Crystal structure of HLA-A2 bound to LIR-1, a host and viral major histocompatibility complex receptor. Nat Immunol. 2003; 4:913–919. [PubMed: 12897781]
21. Cheng H, et al. Crystal structure of leukocyte Ig-like receptor LILRB4 (ILT3/LIR-5/CD85k): a myeloid inhibitory receptor involved in immune tolerance. J Biol Chem. 2011; 286:18013–18025. [PubMed: 21454581]
22. Pulford K, Micklem K, Thomas J, Jones M, Mason DY. A 72-kD B cell-associated surface glycoprotein expressed at high levels in hairy cell leukaemia and plasma cell neoplasms. Clin Exp Immunol. 1991; 85:429–435. [PubMed: 1893623]
23. Allan DSJ, et al. Tetrameric complexes of human histocompatibility leukocyte antigen (HLA)-G bind to peripheral blood myelomonocytic cells. J Exp Med. 1999; 189:1149–1156. [PubMed: 10190906]
24. Brinkman EK, Chen T, Amendola M, van Steensel B. Easy quantitative assessment of genome editing by sequence trace decomposition. Nucleic Acids Res. 2014; 42:e168. [PubMed: 25300484]
25. Garcia KC, et al. An alphabeta T cell receptor structure at 2.5 A and its orientation in the TCR-MHC complex. Science. 1996; 274:209–219. [PubMed: 8824178]
26. Garboczi DN, et al. Structure of the complex between human T-cell receptor, viral peptide and HLA-A2. Nature. 1996; 384:134–141. [PubMed: 8906788]
27. Boyington JC, Motyka SA, Schuck P, Brooks AG, Sun PD. Crystal structure of an NK cell immunoglobulin-like receptor in complex with its class I MHC ligand. Nature. 2000; 405:537–543. [PubMed: 10850706]
28. Sanderson AR. HLA “help” for human B2-microglobulin across species barriers. Nature. 1977; 269:414–417. [PubMed: 71662]

29. Shultz LD, et al. Human lymphoid and myeloid cell development in NOD/LtSz-scid IL2Rγ null mice engrafted with mobilized human hemopoietic stem cells. J Immunol. 2005; 174:6477–6489. [PubMed: 15879151]
30. Mantovani A, et al. The chemokine system in diverse forms of macrophage activation and polarization. Trends Immunol. 2004; 25:677–686. [PubMed: 15530839]
31. Cosman D, et al. A novel immunoglobulin superfamily receptor for cellular and viral MHC class I molecules. Immunity. 1997; 7:273–282. [PubMed: 9285411]
32. Prod'homme V, et al. The human cytomegalovirus MHC class I homolog UL18 inhibits LIR-1^+ but activates LIR-1^- NK cells. J Immunol. 2007; 178:4473–4481. [PubMed: 17372005]
33. Baía D, et al. Interaction of the LILRB1 inhibitory receptor with HLA class Ia dimers. Eur J Immunol. 2016; 46:1681–1690. [PubMed: 27109306]
34. Kim T, et al. Human LilrB2 is a β-amyloid receptor and its murine homolog PirB regulates synaptic plasticity in an Alzheimer's model. Science. 2013; 341:1399–1404. [PubMed: 24052308]
35. Campbell KS, Purdy AK. Structure/function of human killer cell immunoglobulin-like receptors: lessons from polymorphisms, evolution, crystal structures and mutations. Immunology. 2011; 132:315–325. [PubMed: 21214544]
36. Lv Z, et al. Loss of cell surface CD47 clustering formation and binding avidity to SIRPα facilitate apoptotic cell clearance by macrophages. J Immunol. 2015; 195:661–671. [PubMed: 26085683]
37. Garcia-Lora A, Algarra I, Garrido F. MHC class I antigens, immune surveillance, and tumor immune escape. J Cell Physiol. 2003; 195:346–355. [PubMed: 12704644]
38. Challa-Malladi M, et al. Combined genetic inactivation of β2-microglobulin and CD58 reveals frequent escape from immune recognition in diffuse large B cell lymphoma. Cancer Cell. 2011; 20:728–740. [PubMed: 22137796]
39. Zijlstra M, et al. Beta 2-microglobulin deficient mice lack $CD4^-8^+$ cytolytic T cells. Nature. 1990; 344:742–746. [PubMed: 2139497]
40. Koller BH, Marrack P, Kappler JW, Smithies O. Normal development of mice deficient in β2M, MHC class I proteins, and $CD8^+$ T cells. Science. 1990; 248:1227–1230. [PubMed: 2112266]
41. Tseng D, et al. Anti-CD47 antibody-mediated phagocytosis of cancer by macrophages primes an effective antitumor T-cell response. Proc Natl Acad Sci USA. 2013; 110:11103–11108. [PubMed: 23690610]

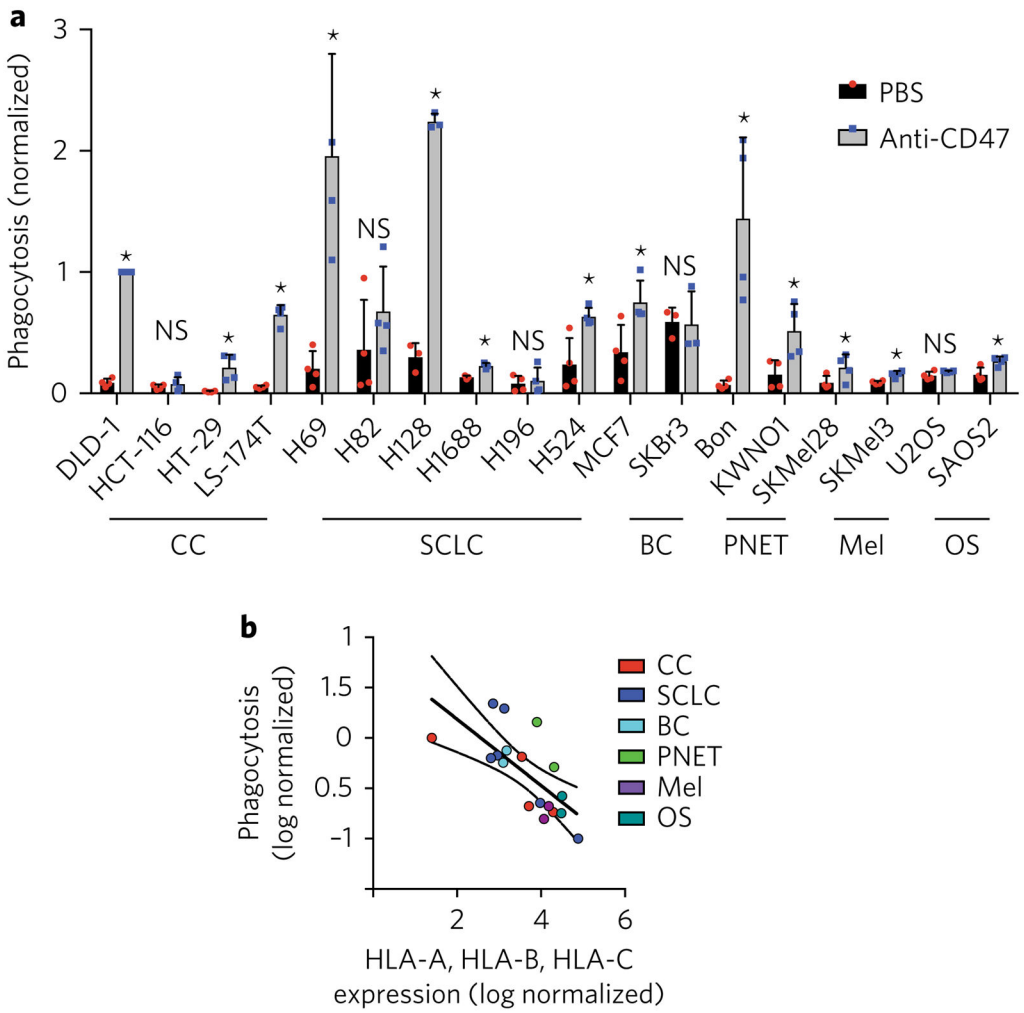

Fig. 1. Resistance to macrophage phagocytosis correlates with MHC class I expression

a, Flow cytometry–based measurement of the phagocytosis of a panel of 18 cancer cell lines (horizontal axis), including colon carcinoma (CC), small cell lung cancer (SCLC), breast carcinoma (BC), pancreatic neuroendocrine tumor (PNET), melanoma (Mel) and osteosarcoma (OS), by donor-derived human macrophages in the presence of PBS or anti-CD47 (key); results normalized to those of DLD1 cells (index control). Each symbol represents an individual donor. Error bars, s.d. of $n = 3$ donors (H128, H1688 and SkBr3 cells) or $n = 4$ donors (all other cell lines). NS, not significant ($P > 0.05$); $*P < 0.05$ (Student's two-sided t-test without multiple-comparisons correction). **b** Phagocytosis induced by anti-CD47 (vertical axis; log-transformed averages of values in **a** plotted against mean fluorescence intensity of MHC class I (horizontal axis): each symbol represents an individual cell line (categories in key); solid diagonal line, best-fit curve; dashed lines, 95% confidence interval ($R^2 = 0.411$; $P = 0.002$ (linear regression t-test)).

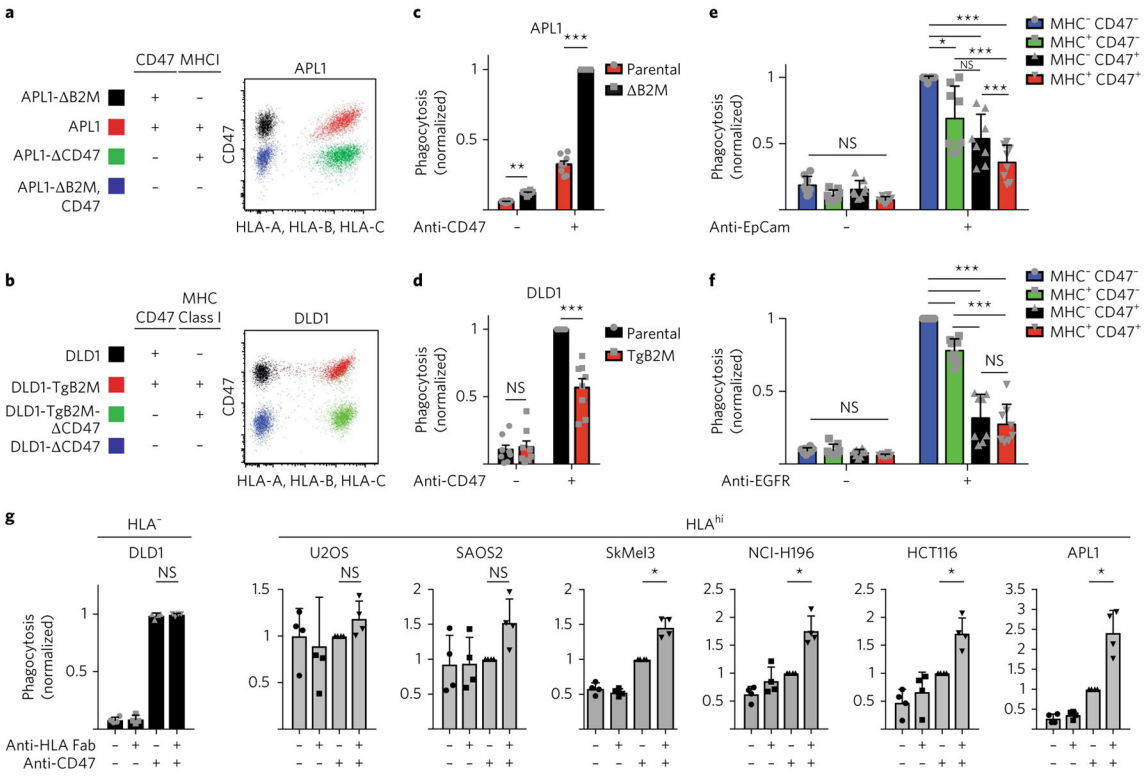

Fig. 2. MHC class I directly protects cells from macrophage attack

a,**b**, Summary (left) of the presence (+) or absence (−) of expression of CD47 and MHC class I (above plot) by APL1 parental cells and genetically engineered sub-lines of APL1 cells lacking expression of β2M (ΔB2M) or CD47 (ΔCD47) or both (ΔB2M,CD47) (left margin) **a** or by DLD1 parental cells and genetically engineered sub-lines of DLD1 cells with transgenic expression of β2M (TgB2M) or lacking expression of CD47 (ΔCD47) or both (TgB2M-ΔCD47) (left margin) **b**, and flow cytometry (right) analyzing the expression of CD47 and MHC class I (HLA-A, HLA-B and HLA-C) by cells as at left (colors in plot match colors at left). **c**,**d**, Flow cytometry–based measurement of the phagocytosis of MHCI $^{+}$ parental APL1 cells and MHCI^{-} (ΔB2M) APL1 cells (key) **c** or of MHCI^{-} parental DLD1 cells and MHCI^{+} transgenic (TgB2M) DLD1 cells (key) **d** by co-cultured human macrophages, in the presence (+) or absence (−) of anti-CD47 (horizontal axis); results normalized to the maximum phagocytosis in each independent replicate experiment. Error bars, s.d. of $n = 8$ donors. **e**,**f**, Flow cytometry–based measurement of the phagocytosis of genetic variants (key) of APL1 cells **e** or DLD1 cells **f** by co-cultured human macrophages, in the presence or absence of antibody to the adhesion molecule EpCam **e** or the epidermal growth factor receptor (EGFR) **f** (horizontal axis); results normalized as in **c**,**d**. Error bars, s.d. of $n = 8$ donors. *$P < 0.05$ and ***$P < 0.001$ (two-way analysis of variance (ANOVA) with multiple-comparisons correction). **g**, Flow cytometry–based measurement of phagocytosis of the MHCI^{-} DLD1 cell line (far left) and the MHCI^{+} cell lines U2OS, SAOS2, SKMel3, NCI-H196, HCT11 and APL1 (middle and right) by donor-derived macrophages, in the presence of various combinations (grid below plot) of antibody to HLA or CD47; results normalized as in **c**,**d**. Error bars, s.d. of $n = 4$ donors. *$P < 0.05$ (Student's

t-test without multiple-comparisons correction). Each symbol (**c**–**g**) represents an individual donor.

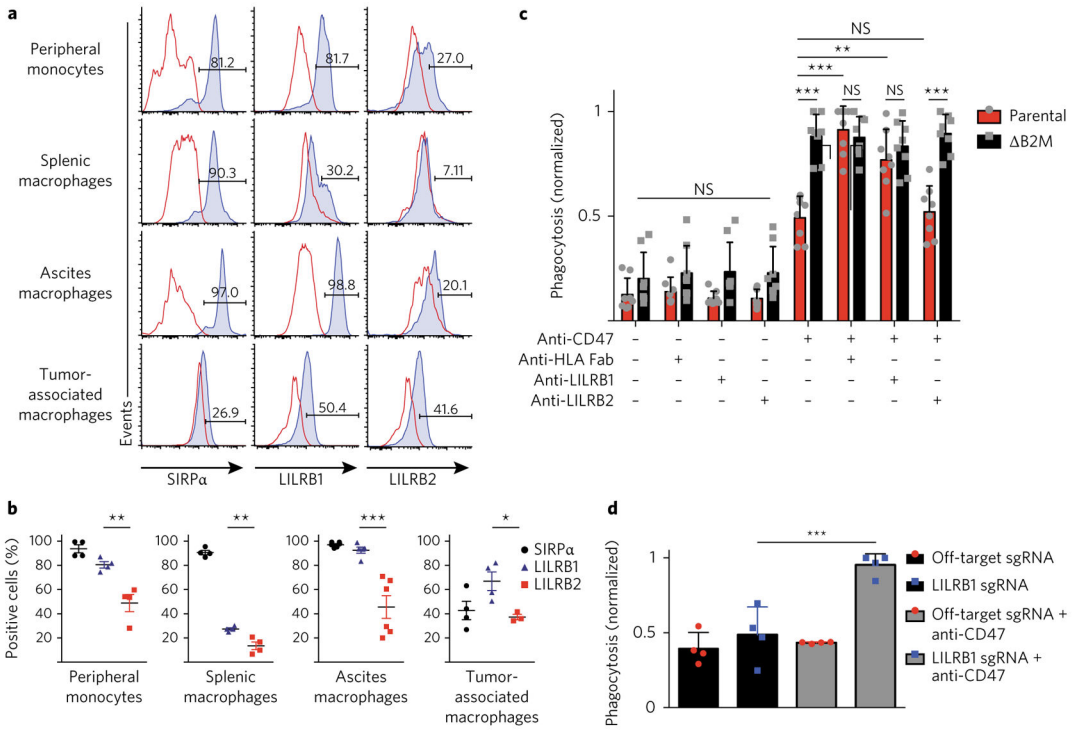

Fig. 3. LILRB1 mediates the detection of MHC class I by human macrophages

a, Flow cytometry analyzing the expression of SIRPα, LILRB1 or LILRB2 (blue shaded curves) by primary human macrophages (left margin); red lines, fluorescence-minus-one control. Numbers above bracketed lines indicate percent cells positive for expression of molecule along horizontal axis. **b**, Frequency of primary monocytes ($n = 4$ donors), primary splenic macrophages ($n = 4$ donors), primary macrophages in ascites fluid ($n = 6$ donors) and primary tumor-associated macrophages ($n = 4$ donors) (below plots) positive for SIRPα, LILRB1 or LILRB2 (key), among total macrophages, as determined by fluorescence-minus-one controls. *$P < 0.05$, **$P < 0.01$ and ***$P < 0.001$ (one-way ANOVA with multiple-comparisons correction). **c**, Flow cytometry–based measurement of the phagocytosis of $MHCI^+$ parental APL1 cells and $MHCI^-$ (ΔB2M) APL1 cells (key) by donor-derived macrophages, in the presence of various combinations of antibodies (grid below plot); results normalized to the maximum phagocytosis in a replicate. Error bars, s.d. of $n = 8$ donors. **$P < 0.01$ and ***$P < 0.001$ (two-way ANOVA with multiple-comparisons correction). **d**, Flow cytometry–based measurement of the phagocytosis of APL1 cells by genetically modified donor-derived macrophages electroporated with off-target sgRNA or sgRNA targeting LILRB1, in the presence or absence of anti-CD47 (key); results normalized as in **c**. Error bars, s.d. of $n = 4$ technical replicates with $n = 2$ donors. ***$P < 0.001$ and ****$P < 0.0001$ (one-way ANOVA with multiple-comparisons correction). Each symbol **b**–**d** represents an individual donor; small horizontal lines **b** indicate the mean (± s.d.).

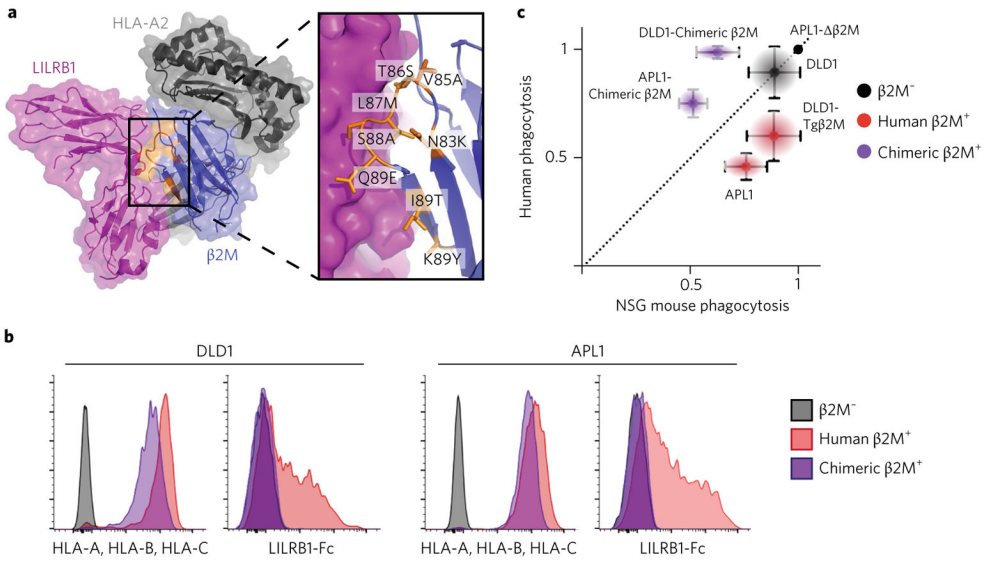

Fig. 4. β2M confers species-specific protection against phagocytosis by macrophages

a, Crystal structure of the LILRB1–β2M–HLA-A2 complex, generated from published structure data (Protein Data Bank accession code IP7Q)[22]; inset, residues within 5 Å of LILRB1 that differ between human β2M and mouse β2M (orange), which were altered (labels in inset) to form a human–mouse chimeric β2M. **b**, Flow cytometry–based measurement of the surface expression of MHC class I (left plot of each pair) and binding of LILRB1-Fc (right plot of each pair) by variants (key) of DLD1 cells (left half) or APL1 cells (right half). **c**, Flow cytometry–based measurement of the phagocytosis of parental MHCI^{-} (β2M^{-}) cells, MHCI^{+} (β2M^{+}) cells or chimeric MHCI^{+} cells (key; specific identification in plot) by co-cultured primary human macrophages (vertical axis) or NSG mouse macrophages (horizontal axis). Vertical error bars, s.d. of $n = 8$ human donors; horizontal error bars, s.d. of $n = 8$ replicates of macrophages pooled from $n = 5$ mice.

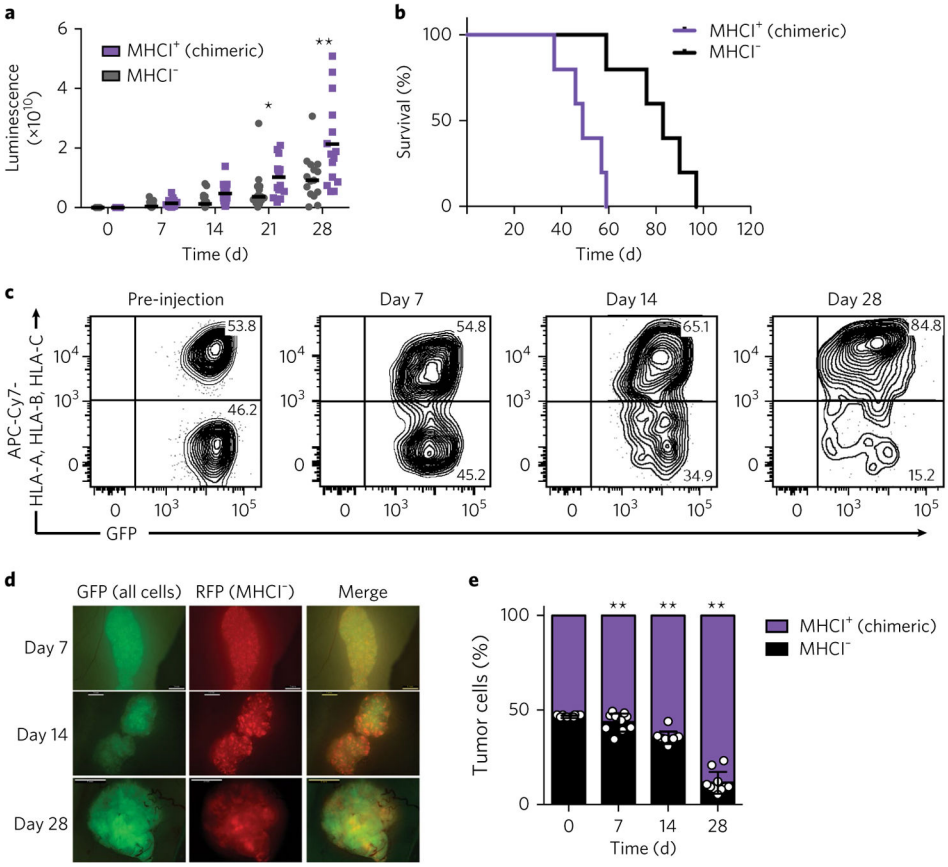

Fig. 5. Expression of MHC class I protects tumor cells from macrophages *in vivo*

a, Tumor bioluminescence (total flux in photons per second) of MHCI^{-} and chimeric MHCI^{+} APL1 cells (key) at various times (horizontal axis) after subcutaneous engraftment into the flanks of NSG mice. Each symbol represents an individual host mouse; small horizontal lines indicate the mean. *$P < 0.05$ and **$P < 0.005$ (two-way ANOVA with Tukey's multiple-comparisons correction). **b**, Survival of NSG mice at various times (horizontal axis) after engraftment of MHCI^{-} or chimeric MHC I^{+} APL1 tumors (key). $P < 0.005$ (Mantel-Cox test). **c**, Flow cytometry analyzing the expression of HLA-A, HLA-B and HLA-C in mixed-chimeric MHC I^{+} and MHC I^{-} DLD1 tumor cells before injection (far left) and in dissociated tumors at days 7, 14, and 28 after injection (above plots) as in **a**. Numbers in outlined areas indicate percent cells in each. **d**, Whole-mount fluorescence microscopy of mixed-chimeric MHC I^{+} and MHC I^{-} APL1 tumors on days 7, 14, and 28 after injection (left margin) as in **a**. GFP, green fluorescent protein; RFP, red fluorescent protein. Scale bars, 1 mm (top two rows) or 5 mm (bottom row). **e**, Flow cytometry–based quantification of the frequency of chimeric MHC I^{+} DLD1 cells and MHC I^{-} DLD1 cells (key) on days 7, 14, and 28 after injection (horizontal axis) as in **a**. Each symbol represents an individual host mouse. Error bars, s.d. of $n = 10$ mice, in two independent experiments. **$P < 0.005$ (two-way ANOVA with Sidak's multiple-comparisons correction).

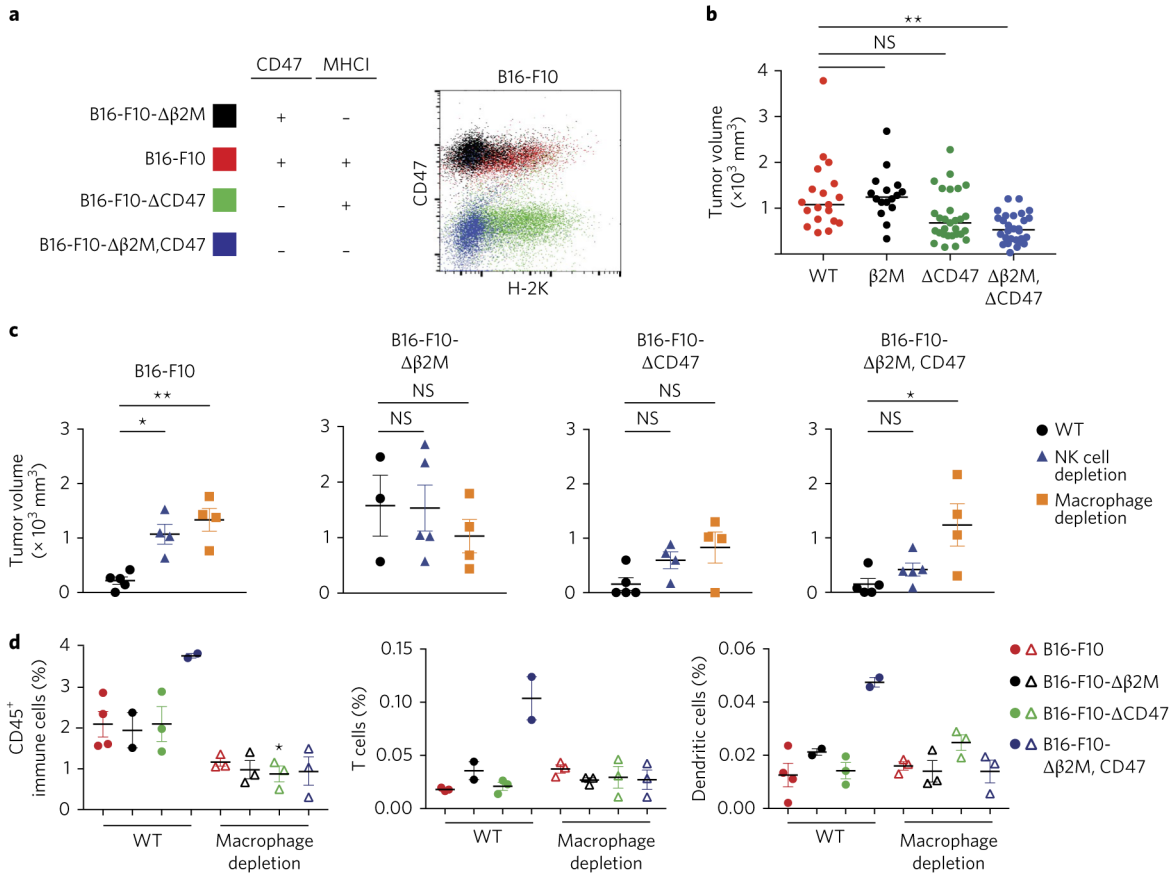

Fig. 6. Expression of MHC class I protects tumor cells from macrophages in a syngeneic, immunocompetent setting

a, Summary (left) of the expression of CD47 and H-2K (MHCI) (above plot) by B16-F10 cells and four genetically engineered sub-lines of B16-F10 cells lacking expression of β2M or CD47 or both (left margin), and flow cytometry (right) analyzing the expression of CD47 and MHC class I (H-2K) by cells as at left (colors in plot match colors at left). **b**, Tumor volume of MHC I^+CD47^+ (WT), $MHCI^-CD47^+$ (β2M), $MHCI^+CD47^-$ (ΔCD47) and $MHCI^-CD47^-$ (Δβ2M,CD47) B16-F10 cells (horizontal axis) 20 d after engraftment into *Rag* $^{-/-}$ *Il2rg* $^{-/-}$ BALB/c mice. $^{**}P < 0.001$ (one-way ANOVA with Tukey's multiple-comparisons correction). **c**, Tumor volume of B16-F10 variants (above plot) 25 d after engraftment into fully immunocompetent C57BL/6 wild-type mice (WT) or C57BL/6 mice depleted of NK cells or macrophages (host, key). $^{*}P < 0.01$ and $^{**}P < 0.001$ (one-way ANOVA with multiple-comparisons correction). **d**, Frequency of all $CD45^+$ immune cells (left), or of T cells (middle) or dendritic cells (right) among $CD45^+$ immune cells, in B16-F10 variant tumors (key) 25 d after engraftment into fully immunocompetent C57Bl/6 wild type mice (filled circles) or C57Bl/6 mice depleted of macrophages (open triangles) (host, horizontal axis).